Annual survey of water vapor behavior from the OMEGA mapping spectrometer onboard Mars Express

Luca Maltagliati, Dmitrij V. Titov, Thérèse Encrenaz, Riccardo Melchiorri, Francois Forget, Horst U. Keller, Jean-Pierre Bibring

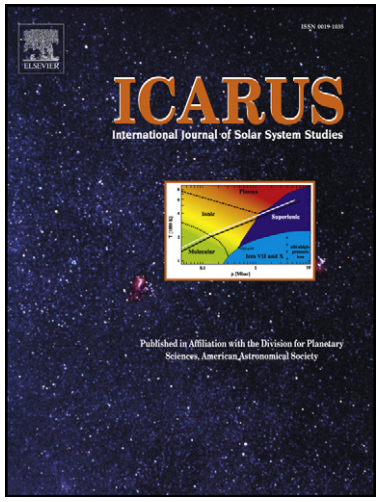

Annual survey of water vapor behavior from the OMEGA mapping spectrometer onboard Mars Express

Luca Maltagliati, Dmitrij V. Titov, Thérèse Encrenaz, Riccardo Melchiorri, Francois Forget, Horst U. Keller, Jean-Pierre Bibring

PII: S0019-1035(11)00121-7
DOI: 10.1016/j.icarus.2011.03.030
Reference: YICAR 9773

To appear in: *Icarus*

Received Date: 29 January 2009
Revised Date: 28 March 2011
Accepted Date: 30 March 2011

Please cite this article as: Maltagliati, L., Titov, D.V., Encrenaz, T., Melchiorri, R., Forget, F., Keller, H.U., Bibring, J-P., Annual survey of water vapor behavior from the OMEGA mapping spectrometer onboard Mars Express, *Icarus* (2011), doi: 10.1016/j.icarus.2011.03.030

Annual survey of water vapor behavior from the OMEGA mapping spectrometer onboard Mars Express

Luca Maltagliati[a,b], and Dmitrij V. Titov[a,c], and Thérèse Encrenaz[d], and Riccardo Melchiorri[d,e], and Francois Forget[f], and Horst U. Keller[a], and Jean-Pierre Bibring[g]

[a] *Max-Planck-Institut für Sonnensystemforschung, Max-Planck Str. 2, 37191 Katlenburg-Lindau, Germany*
[b] *LATMOS, Quartier des Garennes, 11 Boulevard d'Alembert, 78280 Guyancourt, France*
[c] *ESA-ESTEC, Keplerlaan 1, PO BOX 299, 2200 AG Noordwijk, The Netherlands*
[d] *Observatoire de Paris, DESPA Place Jules Janssen, Meudon, 92195 France*
[e] *SRI International, Molecular Physics Laboratory, 333 Ravenswood Av., Menlo Park, CA 94025, USA*
[f] *LMD / CNRS / Universite Paris VI, 4 Place Jussieu, Paris, 75252, France*
[g] *IAS / CNRS / Universite Paris XI, Bat 121, Orsay, 91405 France*

Number of pages: 26
Number of tables: 0
Number of figures: 12

Proposed Running Head:
Seasonal behavior of martian water vapor with OMEGA/MEx

Luca Maltagliati
LATMOS
Quartier des Garennes
11 Boulevard D'Alembert , 78280 Guyancourt, France

Email: luca.maltagliati@latmos.ipsl.fr
Phone:

1. A short review on the martian water cycle

Observation of water in all of its states (solid, liquid, gaseous) has always been a prime objective of ground- and space-based missions to Mars, due to the crucial role of water for the habitability of a planet. After the seminal Viking mission [MAWD instrument, 16], water vapor has been monitored continuously for the last 15 years by three spacecrafts. Mars Global Surveyor (MGS), with the Thermal Emission Spectrometer (TES), covered Martian Years (MY) 24 – 27 [31]. Mars Express, operating since 2004 (end of MY 26), carries three spectrometers with different capabilities that can retrieve water vapor from different spectral signatures. The results of the first martian year of observations have been published by SPICAM, which uses the 1.38 μm band in the near-IR [8], and PFS, that can detect water vapor both in the thermal infrared [PFS-LW, 15] and with the 2.56 μm band [PFS-SW, 41]. Finally, the CRISM instrument on Mars Reconnaissance Orbiter (MRO) is active since the end of 2006 (MY 28) [33]. The measurements from orbit are complemented by a comprehensive set of ground-based observations [i.e. 36, 6].

All these datasets trace a consistent picture. Water vapor is the most variable trace gas in the atmosphere of Mars. This demonstrates its involvement in a variety of physical and chemical processes on the planet. Water vapor variations follow a distinct annual cycle with only minor interannual differences [32]. H_2O abundance fluctuates of almost two orders of magnitude, from 0 to $\approx 60 – 70$ pr. μm, with an annual average of ~ 10 pr. μm. The water cycle on Mars is driven by three main mechanisms: the periodic variations of insolation on the polar caps, that induce a condensation-sublimation cycle; water exchange between the atmosphere and the regolith layer; and planetary circulation, that transports water vapor both at global and at local scales. In the last years, also the role of water ice clouds on the H_2O seasonal cycle has been re-evaluated [4, 26].

This scenario still presents several obscure points. One of the main current controversies concerns the role of regolith. Böttger et al. [3] used a detailed 10-layer regolith model coupled with a General Circulation Model (GCM) to show that an active regolith is needed to reproduce TES observations, otherwise the atmosphere is a factor of 2 – 4 too wet. On the contrary, other recent 3D climatological models suggested that the regolith does not seem to be an important driver of the water cycle [27, 26]. Montmessin et al. [26], in particular, managed to reproduce the observed seasonal behavior without introducing the regolith in the model. Observations give contradictory results as well. Surface-atmosphere coupling was considered to be the main responsible for the water vapor mixing ratio enhancement on the Tharsis volcanoes as observed by ISM/Phobos, according to the 1D model of Titov et al. [40], but recent results by OMEGA suggest that the circulation induced by the local topography is the dominant trigger of this effect [18]. The coincidence of a local maximum of H_2O vapor over Arabia Terra (removing topography effects), found by most instruments, with the water-rich subsurface region detected by Mars Odyssey [23] seems to point at the significance of regolith-atmosphere interactions. However, the comparison between PFS-LW results and GCM simulations supports the hypothesis that these maxima are actually caused by atmospheric dynamics [15]. The importance of water ice clouds is also still unclear. The GCMs of Richardson and Wilson [27] and Montmessin et al. [26] show

that they have the potential to influence significantly water transport, particularly the inter-hemispheric one triggered by the Hadley circulation. Moreover, deposition from clouds both redistributes water vapor vertically [see also 22] and is essential to bring atmospheric water back to the surface in some seasons of the year. It is interesting to remark that these are the same models that reduce the importance of the regolith for the water cycle. It seems that the two effects of regolith and ice clouds cannot be properly discriminated by the observations of the integrated H_2O column density alone.

Our understanding of water vapor behavior on Mars is based mainly on the interpretation of its annual variations, and partially on its spatial distribution. Other important diagnostics have not been used yet up to their potential. The diurnal variability has important physical implications for the martian water cycle, because it gives insight on the relevance of surface-atmosphere interactions on the water cycle. In fact, regolith sorption processes depend strongly on temperature, and therefore on insolation. A significant influence of the superficial layer on the water cycle would produce a symmetric daily behavior centered around noon, as some observations suggest [38, Fig. 4]. However, the measurements are still too sparse to reach a definite conclusion. The datasets show ambiguous results, and recently some Mars Express observations have observed less prominent diurnal variations, without ruling out an active regolith layer [15, 20]. Signatures of significant surface-atmosphere exchange could be detected also by looking at the vertical distribution of water vapor. If a good part of the water desorbed from the regolith in the morning were adsorbed again in the evening, it would not have the time to be distributed uniformly throughout all the atmosphere, and would generate an enrichment within the Planetary Boundary Layer (PBL). More generally, knowledge of water vapor vertical profile is pivotal to determine the relative importance of the various sources and sinks of the H_2O cycle. Through direct measurements of vertical distribution, information regarding the height of the saturation level, and consequently on the temperature structure of the atmosphere and other related phenomena, as delayed condensation, formation of ice particles, and deposition, can also be extracted. Moreover, observations of water in the upper atmosphere are essential to the poorly constrained photochemical models (Krasnopolsky 2006, Lefevre et al. 2008). As for the daily variability, the currently available datasets are very limited. Only ISM/Auguste retrieved direct observations of water vapor, but just for one martian month and with scarce spatial coverage [30]. The analysis of few orbits of SPICAM solar occultations shows strong variations in mixing ratio [9]. A significant advancement in our knowledge of the vertical distribution of water vapor is expected from the full SPICAM dataset, which encompasses more than 3 martian years, and from the submillimeter sampling of the atmosphere from the Mars Climate Sounder (MCS) on MRO [19].

The OMEGA spectrometer aboard Mars Express is particularly well-suited and versatile for the investigation of the water cycle, because it allows both the large-scale global observation and the detailed analysis of specific regions of interest, thanks to its high spatial resolution and mapping capability. Examples of this second approach are the study of the sublimation of the northern polar cap [7] and the focus on the volcanoes of the Tharsis region [18]. In this paper we use the OMEGA instrument to provide a global survey of the annual cycle of water vapor, completing the series of papers from the spectrometers of Mars Express. We present all the various aspects of the cycle, from the yearly trend, to the longitudinal distribution, and the diurnal variability. Information

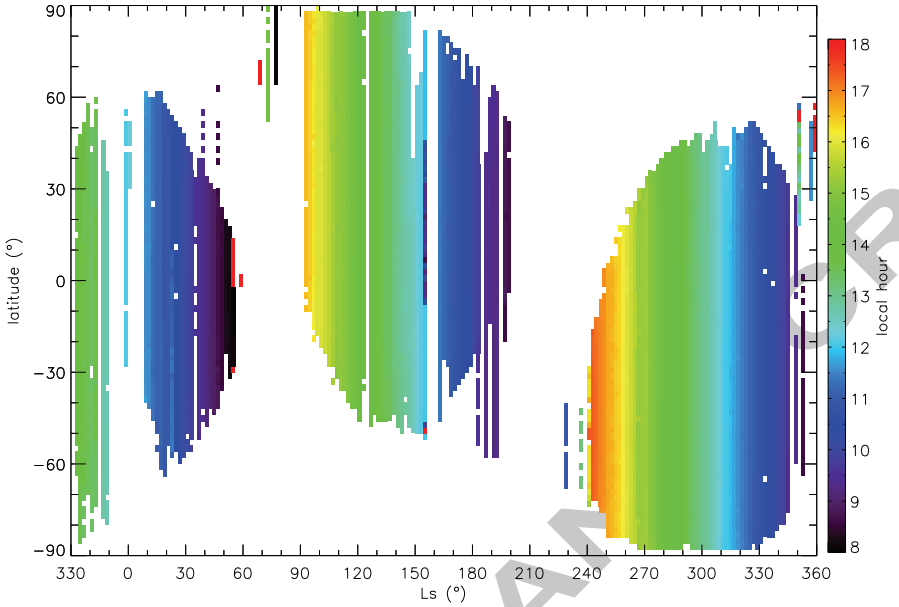

Figure 1: Plot of the distribution of OMEGA orbits in the first martian year, binned 2° in L_s and latitude. The color scale indicates the local hour. The relation between season and local time is evident.

on the H_2O vertical profile during the year is also given, through the determination of its saturation height.

2. The OMEGA experiment

OMEGA (Observatoire pour la Minéralogie, l'Eau, les Glaces, et l'Activité) is the only spectrometer on the Mars Express spacecraft with mapping capability [2]. Its three channels span over the visible and the near-IR part of the spectrum (0.38 – 5.1 μm), with signal-to-noise ratio > 100 over the full spectral range. OMEGA's spectral resolution varies between 7 and 20 nm depending on the wavelength channel. In this work the SWIR-C channel is used, which has a wavelength range 0.93 – 2.73 μm with a spectral resolution of 13 nm. The spatial resolution of the spectrometer goes from $\sim$ 300 m, at pericenter, to 5 km at apocenter. On average, the spatial resolution is 1 – 2 km/pixel, for altitudes between 1500 and 4000 km. Also the full field-of-view of SWIR-C depends on the altitude of the spacecraft over the surface of Mars, and can cover a maximum of 8.8°, which corresponds to a maximum spatial coverage of $\approx 10°$ at the equator. The latitudinal dimension of the mapping is provided by the motion of the orbiter.

This work includes the retrieval of water vapor abundance for the last part of MY 26, from $L_s \sim 330°$ (January 2004 – 5 March 2004) and the whole MY 27 (6 March

2004 – 21 January 2006), covered by the first 2600 orbits of Mars Express. OMEGA was active in 617 of these. Figure 1 displays the evolution of local time of observations over the course of the considered time interval. The whole year is monitored with the exception of two gaps, the end of northern spring ($L_s = 60^\circ - 90^\circ$) and most part of northern autumn ($L_s = 190^\circ - 240^\circ$), due to the interruption of OMEGA activity. Figure 1 shows that the local time is related to season, because of the orbital evolution of the spacecraft. The diurnal variations, thus, cannot be disentangled from the seasonal trend. This means that diurnal variations can introduce a bias in our (and other Mars Express') results, particularly in seasons of low activity. This issue, together with a study on the diurnal variability by OMEGA data, is discussed in more detail in Section 4.3.

3. Data analysis

3.1. Data treatment procedure

The data reduction technique was presented in detail in Maltagliati et al. [18]. Here we summarize the most important points, going into more detail on the few differences that have been introduced. We employ a minimization procedure which finds the best-fit of the synthetic spectrum to the measured one in the 2.6 μm band of water vapor. The only free parameter in this procedure is the mixing ratio of water vapor below the saturation level. We calculate the synthetic spectrum of the band using a fast and accurate line-by-line algorithm which takes into account the contribution of atmospheric CO_2 and H_2O [39]. The synthetic spectrum depends significantly on the climatological parameters, namely the vertical profiles of pressure, temperature, and water vapor. We extract the first two from the Mars Climate Database (MCD), version 4.1 [14], which relies on the LMD-AOPP GCM [13]. The H_2O vertical profile, instead, is computed by our minimization procedure, under the assumptions that it is controlled exclusively by saturation physics and that water is well-mixed below the saturation level [18, Fig. 3]. From a physical point of view this hypothesis implies that, apart from saturation, any effect that can create vertical inhomogeneities in the H_2O distribution is neglected. Thus, either the vertical mixing is more efficient than any local source or sink of water vapor, or these sources/sinks are weakly effective or absent. Our tests show that the assumptions regarding the H_2O vertical profile significantly affect the retrievals [for more details see 18, Section 3.2]. Lacking more direct measurements of water vapor vertical distribution, the use of the well-mixed approximation, supported by few observations [30], is the safest approach to this complex issue.

A raw OMEGA spectrum is treated with a standard procedure to remove first-order instrumental effects, and then it is binned. Here we use a different binning approach compared to Maltagliati et al. [18], because the purpose is different. In the present study we aim at a global survey using all available OMEGA orbits. In order to save computational time, we retrieve only the middle strip of each orbit, binned 10 pixels wide in the longitudinal direction and with a latitudinal binning chosen between 10, 20, 30, and 40 pixels, whichever is the largest number that covers $\leq 1^\circ$. In this way, we do not exploit OMEGA's mapping capability, but we retain a good representation of the latitudinal trend in each orbit. Each binned spectrum is normalized to a continuum.

Unlike Maltagliati et al. [18], we used the triplet (2.514, 2.527, 2.540 μm) instead of the (2.527, 2.540, 2.553 μm) one as continuum reference for the short wavelength wing.

The best-fit is determined by minimizing the mean absolute deviation between the synthetic and the measured spectrum, considering 7 spectral points between 2.527 and 2.605 μm. The two spectels at 2.618 and 2.631 μm, on the right wing of the band, were excluded from the retrieval because of instrumental problems. Integration along the column of atmosphere gives then the column density. This procedure employs absolute spectra and thus avoids any systematic effect related to the choice of a reference normalizing spectrum. Moreover, the best-fit over several spectral points allows us to use both band depth and band shape to determine the water abundance. Figure 2 shows two examples of the 2.6 μm water band as observed by OMEGA in different locations and seasons, together with synthetic spectra computed with various water vapor mixing ratios. The difference in water scenario accounts for the difference in band depth, which varies from $\sim$ 4% to more than 15%. The band depth is dependent mainly on water vapor amount, but the climatological parameters also play a role, pressure in particular.

The mean absolute deviation of the best-fit (σ_{best}) gives a measure of the quality of the fit for each retrieval: the smaller, the better is the fit. Figure 3 shows four examples of retrievals with different quality. When the band is too noisy the result of the fit is just formal, with no physical meaning. For this reason we discard the spectra with $\sigma_{best} \geq 8. \cdot 10^{-3}$ (chosen through visual inspection). The great majority of the retrievals stays within this threshold.

3.2. Computation of the uncertainties

The retrieval uncertainties can be divided into two main categories. The first group is related to the climatological model used to build a synthetic spectrum. The other one is connected to the measured spectrum and its treatment. It consists of the effects of random noise, precision of OMEGA calibration, and influence of continuum.

3.2.1. Uncertainties from the climatological model

The causes of the uncertainties associated with MCD are the low spatial resolution of the model (5.675° $\times$ 3.75°), compared to OMEGA's, and the intrinsic error of the GCM itself. We estimate the first by analyzing some test orbits with the new version of MCD (4.2) which provides atmospheric profiles interpolated at high resolution (1/32°) using MOLA data. We could not use MCD 4.2 for all our retrievals because it was published after a significant portion of dataset had already been processed. The low resolution of MCD accounts for less than 5% of the relative error. Such low value can be explained by the fact that on average the surface of Mars has smooth altitude variations. This result supports our choice to retain the retrievals performed with the previous version of the MCD. This condition fails in the regions of extreme topography like Tharsis, where the error due to the low resolution can increase up to $\approx$ 30% [18]. The general trend is anyway not affected. The most significant uncertainty related to the GCM itself comes from temperature. Typical temperature error is $\sim$ 5 K, with slight variations depending on the local hour [24], and generates a relative error on water retrievals of around 10%. Pressure-related uncertainties are negligible.

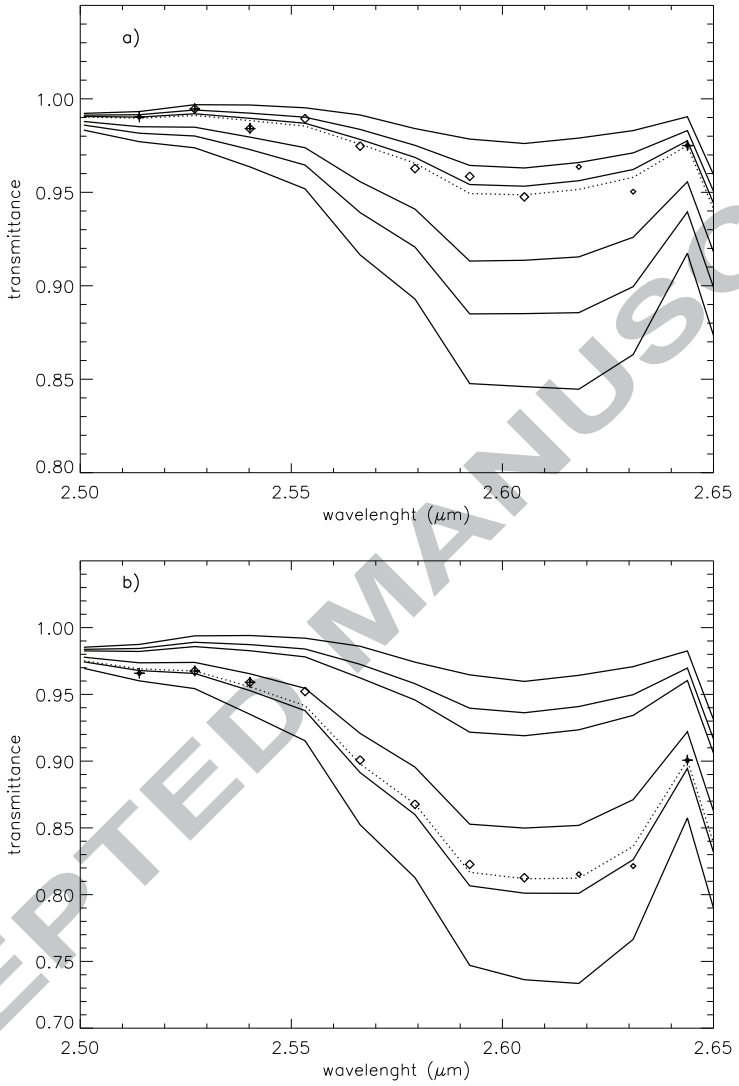

Figure 2: Examples of spectra acquired in two different season. The diamonds indicate the measured spectrum. The bigger diamonds are the spectel used for the best-fit. The spectels marked with a cross are the continuum reference. The solid lines are synthetic spectra with six different values of water vapor mixing ratio (from top to bottom: 10, 50, 100, 500, 1000, and 2000 ppm). (a): L_s = 16.0°, (17.5°S, 154.1°E), H_2O mixing ratio = 130 ppm, 6.4 pr. μm. (b): L_s = 115.2°, (81.0°N, 284.4°E), H_2O mixing ratio = 872 ppm, 62.7 pr. μm.

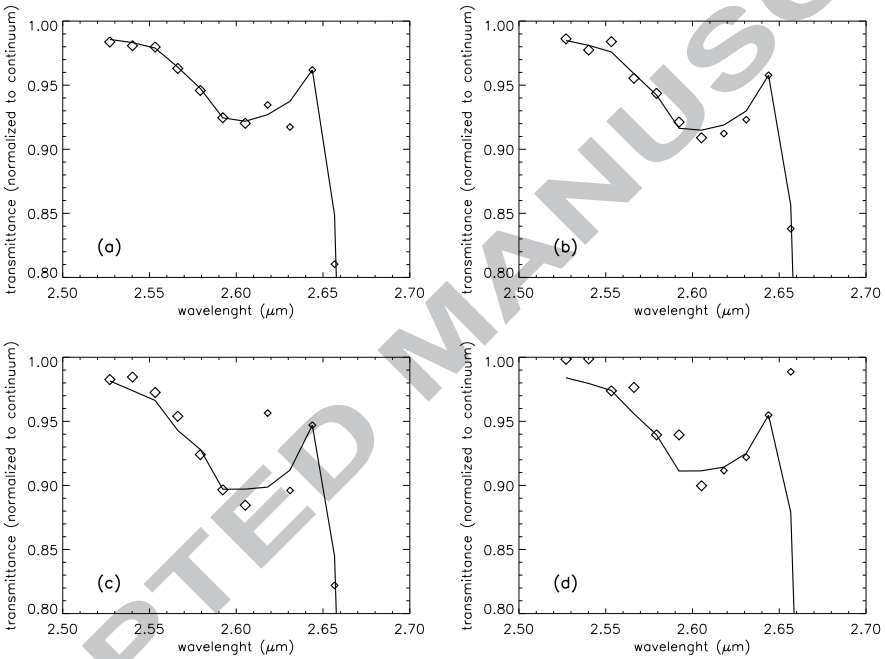

Figure 3: Four examples of best-fit results with different quality levels. (a) excellent fit ($\sigma_{best} = 1.24 \cdot 10^{-3}$); (b) typical good fit ($\sigma_{best} = 4.04 \cdot 10^{-3}$); (c) acceptable fit ($\sigma_{best} = 6,48 \cdot 10^{-3}$); (d) bad fit ($\sigma_{best} = 13.5 \cdot 10^{-3}$).

The presence of dust affects the temperature profile of the atmosphere, as well as the H_2O band depth through scattering and extinction processes. We use as first order correction the dust scenario included in MCD that is derived from TES observations of MY24, a year supposed to be typical in dust activity with no global dust storms. This choice is supported by observations of dust seasonal behavior during MY27. The uncertainty due to the climatic effects of dust is included in the intrinsic MCD error, described above. The influence of dust on the spectral band is more complex to assess. Few studies treated this effect in detail. We can refer to Encrenaz et al. [5], which presented the results of the radiative transfer modelling of the same water band as observed by OMEGA. They found that the aerosol scattering lowers the 2.6 μm band depth by $\sim 2-8\%$ for $\tau = 0.5-1.0$ for a broad range of H_2O mixing ratios. However, extending these results to our case is not straightforward, because of the differences in the retrieval method and because they made the computations only in the specific case of Hellas Basin. A more complete investigation was performed by Fedorova et al. [10, 11] on the 1.38 μm H_2O band used by the MAWD instrument. They showed that the dust influence, for a fixed optical depth, depends significantly on airmass. In the airmass range of our observations, the H_2O column density retrieval is significantly affected only when the visible dust opacity is larger than $1-1.5$, not expected outside dust storms. Our results should be even less sensitive to dust loading, due to the different wavelength range. In conclusion, we think that the dust uncertainty is small compared to other contributions. Ice clouds have an effect on the spectra similar to dust, changing the band depth through absorption and scattering. Ice clouds are also more directly involved in the water cycle through condensation and deposition effects [28, 26]. However, due to their low optical depth even in the period of higher activity (as the Aphelion Cloud Belt) and their sparse presence, both in space and in time, their influence on our retrievals can be neglected.

3.2.2. Error due to the fitting procedure

The degree of freedom on the choice of continuum in the blue wing introduces a relative error of $\sim 10\%$ on the retrievals. The other contribution of the retrieval method to the error is the noise in the counts of individual spectels. The purely statistical noise of OMEGA on each spectel signal is 1.85 Digital Numbers (DN), regardless of the incoming flux. The averaging of large number of spectra (80 to 400) gives a standard deviation close to 1%, independently of the dimension of the binning. This results confirms that the noise does not behave according to the Poisson statistics, as it should be expected by a read-noise limited instrument like OMEGA. It tells also that the influence of small-scale H_2O fluctuations, unresolved inside the binning domain, is negligible. We made a series of tests running the retrieval procedure on synthetic spectra perturbed by 1% noise. The relative uncertainty on column density is quite uniform for the analyzed orbits, between 10% and 15% on average. There is a weak anticorrelation with the reference values: the lower the unperturbed column density, the higher the relative error. The reason for this anticorrelation is intuitive: for low column densities the band is shallower and thus more sensitive to noise fluctuations. There is not, however, a significant correlation with surface altitude (pressure), which also affects the band depth. A slight anticorrelation between relative error and altitude is present, but only in some orbits and only above ~ 5 km. It possibly depends on local

Cause of uncertainty	column density error (%)
MCD low resolution	5
MCD intrinsic uncertainty	10
spectrum noise	10 – 15
continuum	10

Table 1: Summary of all the significant relative uncertainties on our water vapor retrievals.

effects.

Table 1 sums up the various contributions to the relative error on our retrievals. Considering them independent from each other, the total relative error is about 20%.

4. Results

4.1. The seasonal cycle observed by OMEGA

We applied our retrieval method to the whole dataset, binned each 2° in latitude and L_s as for TES [31]. Figure 4 shows that the number of retrievals included in each bin is highly variable, going from a few digits to $\sim$ 80. The higher the number, the more representative of the average trend is the retrieved H_2O abundance. When the averaged spectra are few, the result can be more susceptible to individual retrievals. The presence of the oblique strips in Fig. 4 is due to the orbits' division in cubes and to the change of width of the OMEGA swath. Between the end of a cube and the beginning of the next one, a small latitude interval is not covered by observations. The position of the gaps between the cubes slowly drifts, following the evolution of the pericenter position with time, and generates the pattern of Fig. 4.

The mean value of the column density in each bin is plotted in Fig. 5 with respect to L_s and latitude. The main features of the cycle, known from the observations by several instruments (listed in Section 1), are well represented. The maximum of activity happens during the northern summer and has already begun when OMEGA starts acquiring data again at $L_s = 90°$, after the gap during northern spring. The few orbits acquired in the period between $L_s = 60° - 90°$ hint at a beginning of the sublimation from the seasonal cap at $L_s \sim 75°$. The global maximum, of $\sim$ 50 pr. μm on average, is reached at $L_s = 100° - 120°$ at latitudes $\sim 55° - 80°$ N, with the highest value of 60.7 pr. μm at $L_s = 102°$ and latitude 78° N. The peak starts decreasing quite abruptly at all polar latitudes down to $55° - 60°$ N, and at $L_s = 140°$ is already extinguished. The string of high values extending down to $\sim 35°$ observed at $L_s = 122°$ is actually due to a selection bias, because it includes a series of orbits passing over Chryse Planitia. During summer and beginning of autumn the local maximum progressively drifts equatorwards. After $L_s = 150°$ the main gush of water vapor is already exhausted, but the drifting local maximum towards lower latitudes persists at least until $L_s = 200°$, when OMEGA has a break in the observations. An increase of water vapor amount at equatorial latitudes starting at $L_s \sim 180°$ can be noticed. During southern late spring

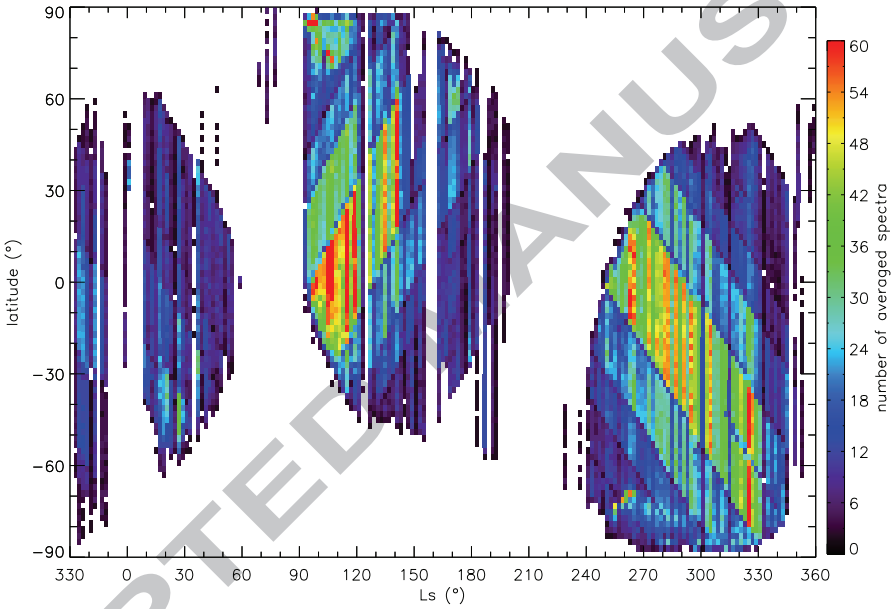

Figure 4: Number of averaged retrievals for each binning domain. The oblique lines are generated by the gap between two adjacent cubes of the same orbit (see text for explanation).

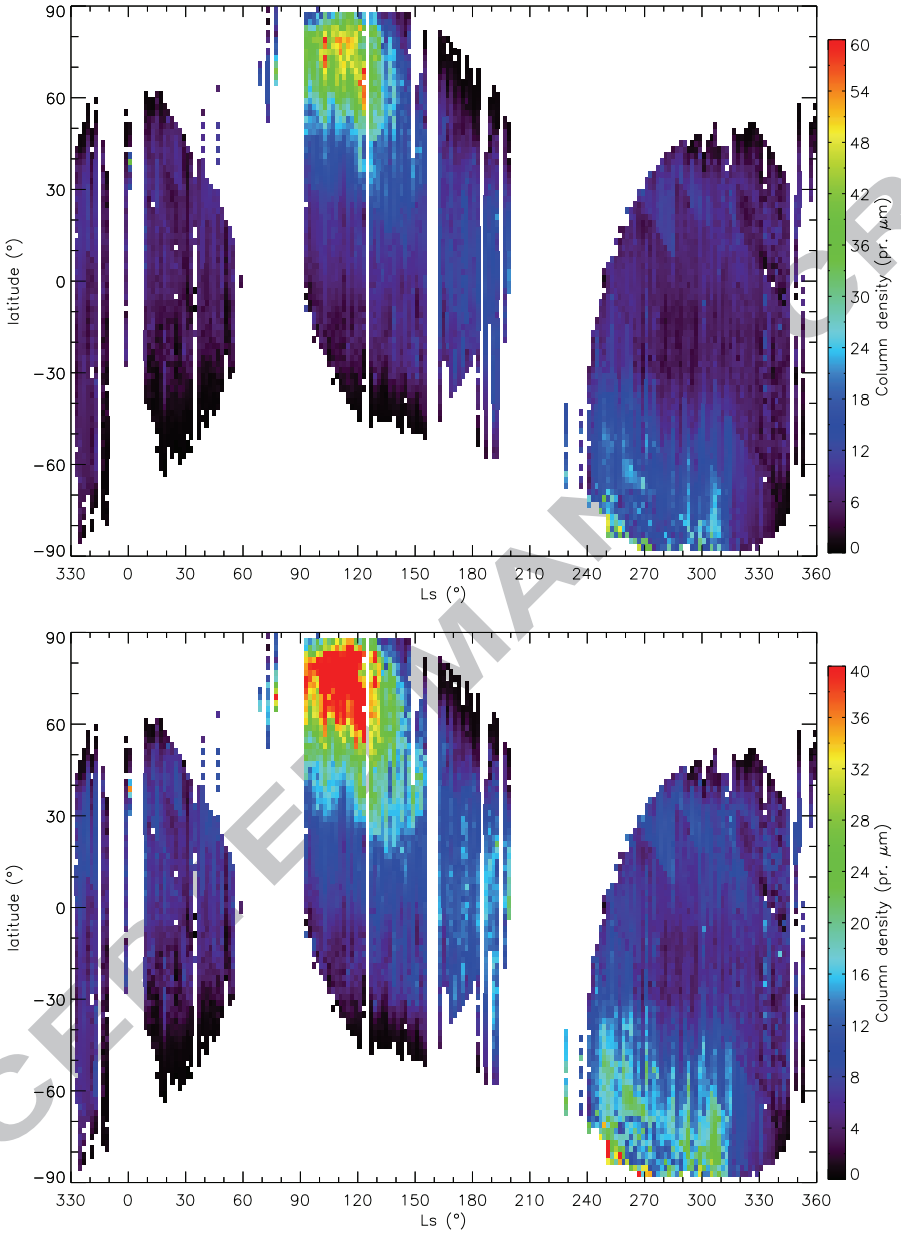

Figure 5: Seasonal behavior of water vapor in martian atmosphere as observed by OMEGA, during the first martian year. The two plots differ in the color scale of H_2O column density. The top plot covers more or less the annual fluctuation of water vapor, from 0 to 60 pr. μm. The bottom plot, up to 40 pr. μm, is provided to stress the secondary features.

and summer a maximum at high southern latitudes seems to begin at $L_s = 245°$, just after OMEGA started to acquire data again, but it cannot be inferred clearly by the retrievals whether it had already begun before or not. This maximum has a quite irregular and loose structure, with two relative maxima of ~ 25 pr. μm at $L_s = 260° - 270°$ between $60° - 65°$ S, and on the polar region at $L_s = 300° - 310°$. Compared to the northern summer maximum, the southern one is significantly less intense, around 20 pr. μm on average, and less compact. Its edge is at $\sim 35°$ S at the beginning and it moves slightly towards the pole down to $\sim 50°$ S with the progression of the season. At $L_s = 315°$ the southern maximum ends suddenly, with no signatures of transport. During this season, the behavior outside the area affected by the southern cap sublimation is quite undistinguished. A local minimum between $L_s = 270° - 300°$, that can be associated to the "Low Southern Latitude Summer Minimum" [29, 36], can be noticed. There are also hints at an increase of water vapor abundance on the northern tropical regions. However, our data exhibit here significant scattering, and we cannot draw any firm conclusion on the detection of these features and their physical meaning. After the sharp end of the southern maximum, the water cycle enters the phase of minimum annual activity around the northern spring equinox.

The average column density for the whole dataset is 9.7 pr. μm. The asymmetry between the two hemispheres is evident when we compute their average values separately: 11.8 pr. μm for the northern hemisphere, 8.0 pr. μm for the southern one.

4.2. Comparison with the other datasets

It is important to put our results in the context of the past and simultaneous observations of the water cycle.

4.2.1. Earlier instruments: TES and MAWD

The MGS/TES retrievals are still the longest record of continuous monitoring of atmospheric water vapor on Mars. TES covers up to the beginning of MY 27, meaning that we have simultaneous measurements of the two instruments only for a limited time. For the comparison we use the closest complete Martian Year, MY 26. The small interannual variability of the water cycle [32] and a similar annual dust cycle between MY 26 and 27 minimize the differences between the two martian years. We use the reprocessed TES dataset, which gives column densities $\approx 30\%$ lower compared to Smith [31] and Smith [32] (Smith, private communication).

OMEGA reproduces all the main features of the H_2O cycle observed by TES, with the possible exception of the local maximum at northern tropical latitudes during the southern summer. The quantitative agreement is also quite good (Fig. 6). TES is on average higher than OMEGA, but only by few precipitable microns – the actual average difference on the whole dataset is +0.95 pr. μm – with a more consistent discrepancy at both polar regions during the local summer and at the equator during northern summer. The fine structure of both polar maxima is different. OMEGA northern summer maximum is shorter in time but more extended in latitude, appearing more circular than the TES one. Figure 6 shows that this is the season where the highest absolute difference between the two datasets is concentrated, both towards the negative and the positive extreme. More in detail, the blue area between $55° - 70°$ N at early northern summer

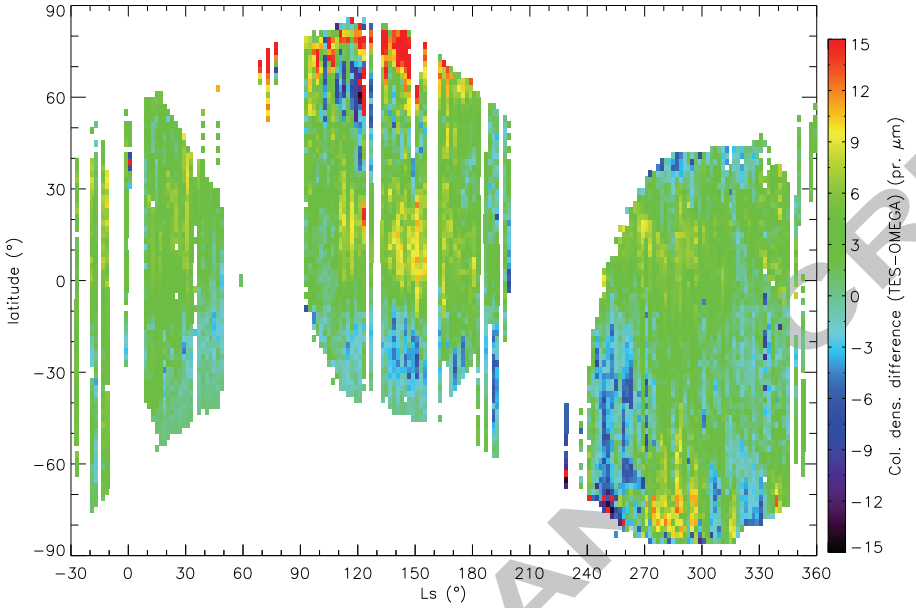

Figure 6: Absolute difference between TES and OMEGA column density.

remarks the larger latitudinal extension of the peak detected by OMEGA with respect to TES, while the red region between $L_s = 130° - 150°$ and the few orbits at mid-end of spring indicate the more abrupt appearance and ending of the OMEGA maximum. The southern summer maximum is significantly different. In the TES results it resembles the northern one, just less intense and with a sharper end, and does not show the two maxima structure that can be seen in OMEGA. In fact, the period of low water vapor that is present in OMEGA between $L_s = 270° - 290°$ almost coincides with the local TES maximum. The discrepancy in water abundance at the poles between TES and OMEGA can have a physical explanation. Tschimmel et al. [41] suggests that the difference of a factor 1.5 – 3 in the retrievals between the reflected and the thermal IR channels of PFS is due, at least for the northern summer maximum, to an enhanced concentration of water vapor near the surface with respect to the commonly assumed vertical distribution (Section 3.1). This hypothesis seems to be confirmed by atmospheric measurements from the Phoenix polar lander [37]. The difference in shape of the southern maximum, however, is more difficult to explain just with a tuning of the vertical distribution.

Less evident differences appear at equatorial-tropical latitudes. The equatorward transport during the northern summer is less pronounced in OMEGA, and the local maximum between 0° – 30° N during southern summer is stronger and more structured in TES. This underestimation of water vapor column density at equatorial latitudes in OMEGA results seems to be a constant behavior during the whole year. By contrast, water vapor amount in the southern hemisphere is generally higher in OMEGA, with

the exception of the summer maximum between $L_s = 270^\circ - 300^\circ$.

To conclude with TES, it is interesting to point out two minor features seen by both datasets. The first is the onset of the equatorward transport at $L_s = 120^\circ$. Both dataset experience relatively high H_2O abundances which suddenly reach down to 30° N. The second is the abruptness of the interruption of the southern maximum at $L_s = 320^\circ$, which happens almost simultaneously for the two instruments, despite the fact that we are observing two different martian years. A possible explanation can be the onset of a particularly strong dust activity, which is indeed observed in the TES case [34]. The dust optical depth monitored by the Mars Exploration Rovers, especially Opportunity, exhibits an increase at the same L_s [35], suggesting that a similar event occurred in MY27 too. Given that the thermal infrared bands are insensitive to dust loading, this explanation implies that the decrease is connected to some physical effect. This would mean that the coupling between the climatic cycles of water and dust is stronger than currently considered. This topic requires a dedicated study which is beyond the purpose of this paper.

The other historical dataset is the one extracted from the MAWD instrument onboard the Viking orbiters. The results published by Jakosky and Farmer [16] are currently outdated. Fedorova et al. [12] demonstrated that the values change significantly if the data are reprocessed using up-to-date spectroscopic and climatologic models. The revisited MAWD data published by Fedorova et al. [12] presents a good agreement with OMEGA, which is on average wetter, but within the uncertainties. It is interesting to notice that the MAWD northern summer maximum is very close to OMEGA, with a very abrupt ending around $L_s = 120^\circ$, in contrast with the more regular behavior seen by TES. The MAWD data of the southern summer are strongly influenced by the global dust storm that happened in MY 12 and cannot be directly compared. The reanalysis of MAWD data with a radiative transfer model to take this effect into account was performed by Fedorova et al. [11] and hints at a TES-like behavior, but this reanalysis was done with the old spectroscopic and climatologic references.

4.2.2. Simultaneous retrievals: SPICAM and PFS

The comparison with the other Mars Express spectrometers has the advantage that water vapor is retrieved in the same year, season and local hour. The instruments, however, look at different water vapor bands. While PFS-SW uses our same band [41], SPICAM employs the 1.38 μm one [incidentally, the same as Viking/MAWD, 8] and PFS-LW the thermal part of the spectrum in the interval 305 – 505 cm^{-1} [15]. Figures 7 – 9 plot the column density absolute difference with OMEGA (with SPICAM, PFS-SW and PFS-LW respectively), using the same color scale of Fig. 6 for better comparison. As for TES, there is good qualitative agreement between all the datasets. Quantitatively, the difference is within the uncertainties for most of the year, but few parts, especially around the northern summer maximum, are more discrepant.

The shape and evolution of the northern maximum as observed by SPICAM is remarkably similar to OMEGA even in the details, as for example the local increase at $L_s \sim 120^\circ$ between $55^\circ - 70^\circ$ N. The evolution of the local maximum towards the equator during northern summer is the same for both instruments. SPICAM sees the equatorial increase at $L_s \sim 180^\circ$ too. The main difference is in the shape of the southern maximum. SPICAM is closer to TES, with one single peak between $L_s = 270^\circ - 300^\circ$

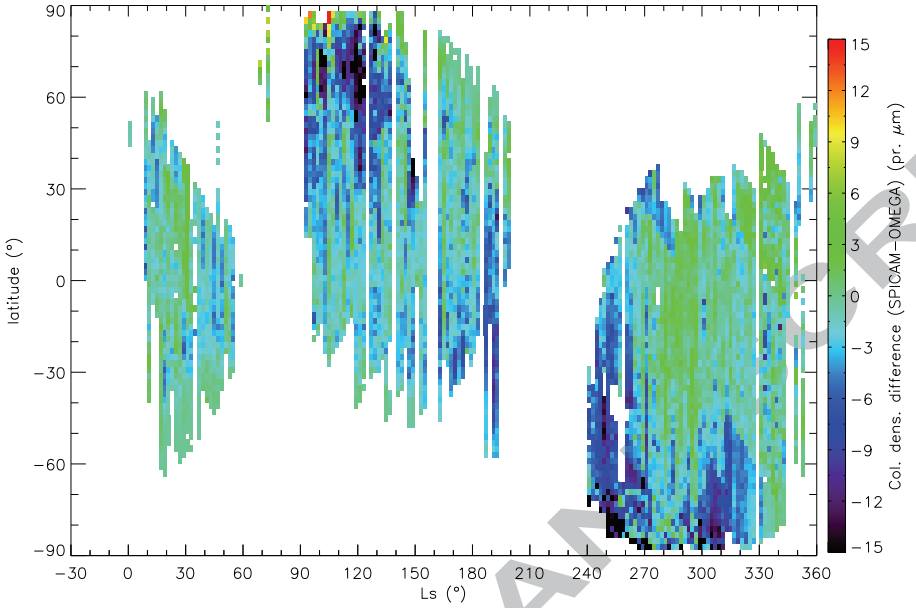

Figure 7: Column density absolute difference between SPICAM and our results.

instead of the two maxima. Regarding absolute quantities, the SPICAM water cycle is, on average, drier. The only period during which SPICAM has persistently more water than OMEGA is between $L_s = 270° - 300°$. The difference is within $^{+1}_{-3}$ pr. μm for most of the year, but it can be higher than 10 μm, always in favor of OMEGA, during both summer maxima.

The PFS data are limited to the first part of the year, until $L_s \sim 200°$, due to instrumental problems. The two channels, while consistent qualitatively with each other, show significant discrepancies in the measured quantity of water vapor in the atmosphere (the factor of 1.5 – 3 mentioned in Section 4.2.1). Figures 8 and 9 show the difference between these two datasets and OMEGA. PFS-SW results are particularly interesting because both the same water vapor band and a very similar retrieval method were used, so the difference in data reduction is minimal. PFS-SW is wetter than OMEGA. If we exclude the strips around $L_s = -10°$ and 190°, that are contaminated by noisy spectra in PFS data, the difference is contained within 2 – 3 pr. μm, apart from the period around the northern maximum. PFS-SW does not see the sudden increase of water vapor towards lower latitudes between $L_s = 120° - 130°$, and it finds more water than OMEGA during the bulk of the maximum at the peak of activity. Finally, PFS-LW retrieves the driest water cycle between all the datasets. It finds a very weak influx of vapor from the northern polar cap sublimation into the atmosphere, and a consequently weak equatorward transport during northern summer. This is the reason of the strong quantitative difference from OMEGA around the maximum, the highest between all the datasets: almost 20 pr. μm. The transport signature also is significantly

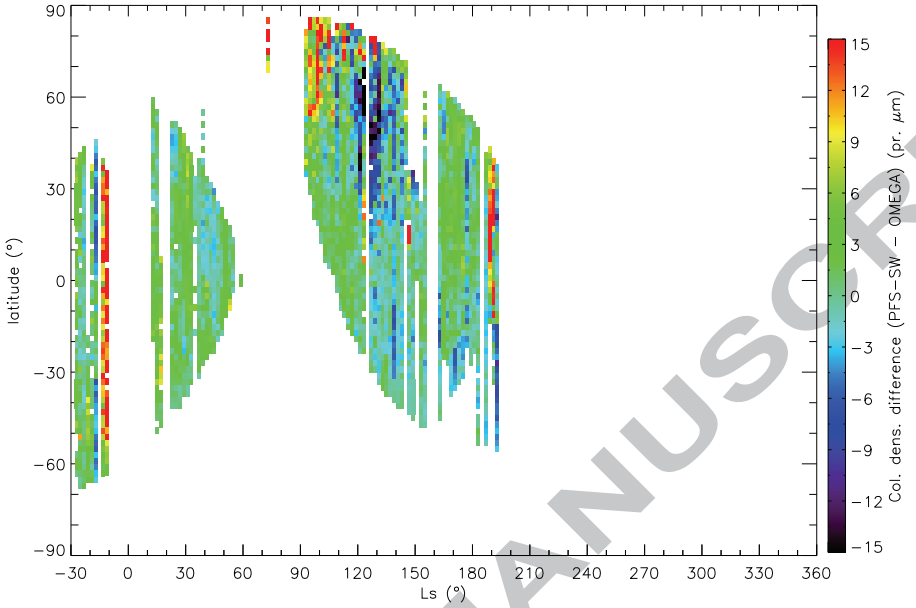

Figure 8: Column density absolute difference between PFS-SW and our results.

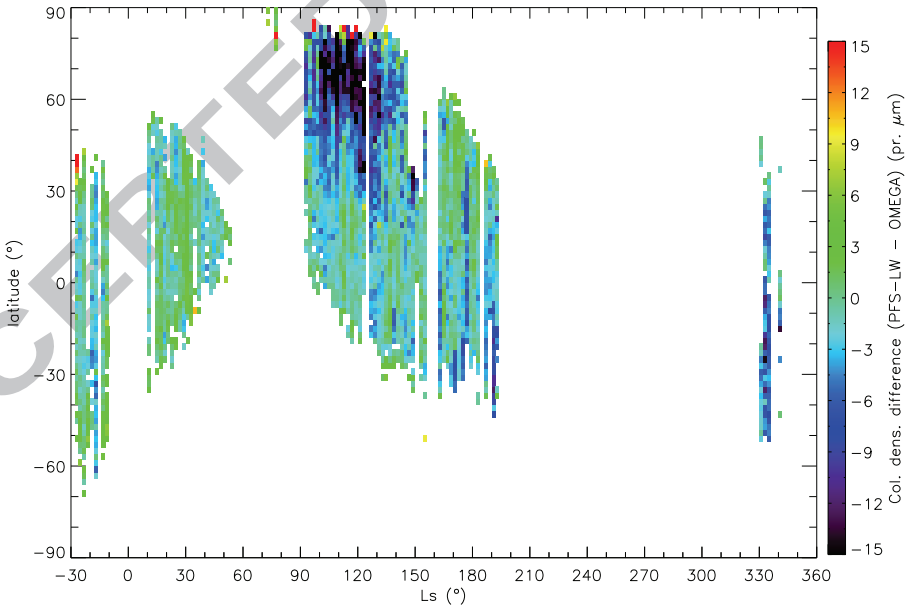

Figure 9: Column density absolute difference between PFS-LW and our results.

lower. In general, PFS-LW is the most distant instrument from OMEGA in terms of quantity of water vapor in the atmosphere. On the contrary, the qualitative agreement is quite good: the whole behavior of the drifting maximum during northern summer is an example. The known features of the water cycle are present but subdued in the PFS-LW retrievals. It is interesting to notice that the equatorial increase of vapor at $L_s \sim 180^\circ$ seems to be a robust feature of all Mars Express datasets. The cause for this increase, which has no counterpart in the MGS and MAWD observations, is not clear. We can probably exclude instrumental effects, though, because of its ubiquitous detection.

4.3. Diurnal variability

Mars Express does not allow direct measurements of daily variations of water vapor, because the local hour of observation is linked to season, with the exception of the polar regions where different local times can be covered by a single orbit [20]. Nevertheless, it is possible to get some information regarding the diurnal variability at a global scale by comparing our results with the TES ones. TES was observing only at 14:00 and 2:00 (but the night observations were not used for the retrieval of water vapor). Thus, for the same L_s we have the observation at 14:00 from TES and another one at varying local time, between 8:00 and 18:00, from OMEGA. According to some in-situ measurements, water vapor reaches its daily maximum around the time of TES observations and a significant decrease both towards the morning and the evening hours [38, Fig. 4]. The daily fluctuations can reach 10 pr. μm. Measurements in the northern polar summer by Phoenix are of this order of magnitude [37]. If this were the case everywhere, we should see a correlation between the hour of Mars Express observations and the difference between TES and OMEGA column density. In particular, we expect this difference to be highest in early morning and late afternoon, and decrease towards noon. A comparison between Figs. 1 and 6 shows clearly that such a correlation does not exist.

This is not, of course, the definite proof that there is no diurnal variation in atmospheric water. The local hour is not the only parameter that differs between TES and OMEGA observations; the comparison is even between two different martian years. However, a diurnal variability of $\sim$ 10 pr. μm should be visible, even taking into account all the possible sources of discrepancy between the two datasets. It must be noted that a daily variation is possibly influenced by local characteristics. In particular, the regolith composition determines the adsorption properties of the soil subjected to insolation. However, diurnal variations do not seem to affect the water cycle on a large scale. This test can be considered a constraint condition for the diurnal variability, which probably does not exceed few precipitable microns. Incidentally, this implies that the seasonal behavior observed by Mars Express instruments well represents the general properties of the global water cycle.

4.4. Spatial variations

We studied the spatial distribution of water vapor on Mars using a 2° latitude – 4° longitude binning. To the first order, water vapor column density depends on topography (that is, surface pressure). We multiplied the column density by the factor $(6.1/P_s)$

to take the topographic influence out of the picture. Figure 10 presents four maps corresponding to different seasons, while Fig. 11 sums up all the orbits of the first martian year.

The maps show that the strongest signatures in the spatial distribution of water vapor are linked to the seasonal effects of sublimation from the polar caps. There are no strong variations in the seasonal maps on the area outside the poles, between -50° and $+50^\circ$ latitude. A maximum on the Tharsis region is visible during all seasons, with some variations in shape. During the spring equinox season higher values are actually found south-west of Tharsis, around Syria Planum, but there is significant scattering and the Tharsis area is only partially covered. In the summer maps the Tharsis maximum seems to stretch also towards Valles Marineris, and in winter it is present along the whole longitude strip, regardless of the latitude. A second maximum over Arabia Terra is less defined and more variable. It is evident at the spring equinox and in late summer (even if there are not many orbits in this season), while in early summer and winter the data are more scattered, and above-average values seem to concentrate on the borders of the Arabia region, at longitude 0° and 60° W, with a "hole" in the middle. The results are however too scattered to speak of seasonal variations in the longitudinal distribution. The scattering does not allow to detect other seasonal secondary maxima either. The only other feature that can be seen in more than one season is a local maximum over Elysium Mons, much less prominent than the other two. Indeed, the most persistent feature in the longitudinal maps is not a maximum, but the slightly curved minimum between $\sim 60^\circ - 30^\circ$ W and $-50^\circ - +30^\circ$ N.

The annual average map (Fig. 11) exhibits similar trends. The most prominent maximum outside the polar regions is around the Tharsis region, extended in latitude and covering also part of Valles Marineris. Another maximum on Arabia Terra can be noticed, but is not so marked compared to its surroundings. The extensive minimum region described above is in between. A weaker maximum over Elysium Mons can be noticed too. The two maxima over Tharsis and Arabia Terra are present in most of the other water vapor datasets, usually more prominently than in our maps [e.g. TES, 31]. The behavior over the poles, which are observed only during their local summer, does not exhibit any significant trend, but some inhomogeneities can be noticed. For example, there are hints at a minimum of activity in the north between $-20^\circ - +20^\circ$ E compared to the surroundings, and in the south around 60° E. Also, a strong compact maximum emerges at $90^\circ - 50^\circ$ E and at $45^\circ - 90^\circ$ E. The polar distribution matches well the results of PFS-SW [41] and Melchiorri et al. [21], who employed OMEGA data to map the summer sublimation.

4.5. H_2O saturation level

The other output of our retrieval method is the height of the saturation level of water vapor (Fig. 12). Saturation follows a clear seasonal pattern, which is strictly dependent on the variations of insolation along the martian year. During northern spring and summer, when Mars is close to aphelion, temperatures and consequently the saturation vapor pressure are lower. The saturation level is closer to the surface. Around perihelion (northern fall and winter) the opposite behavior is expected and indeed observed. The saturation height is also positively correlated with the amount of water vapor in the atmosphere: the more vapor there is in the atmosphere, the closer to the surface

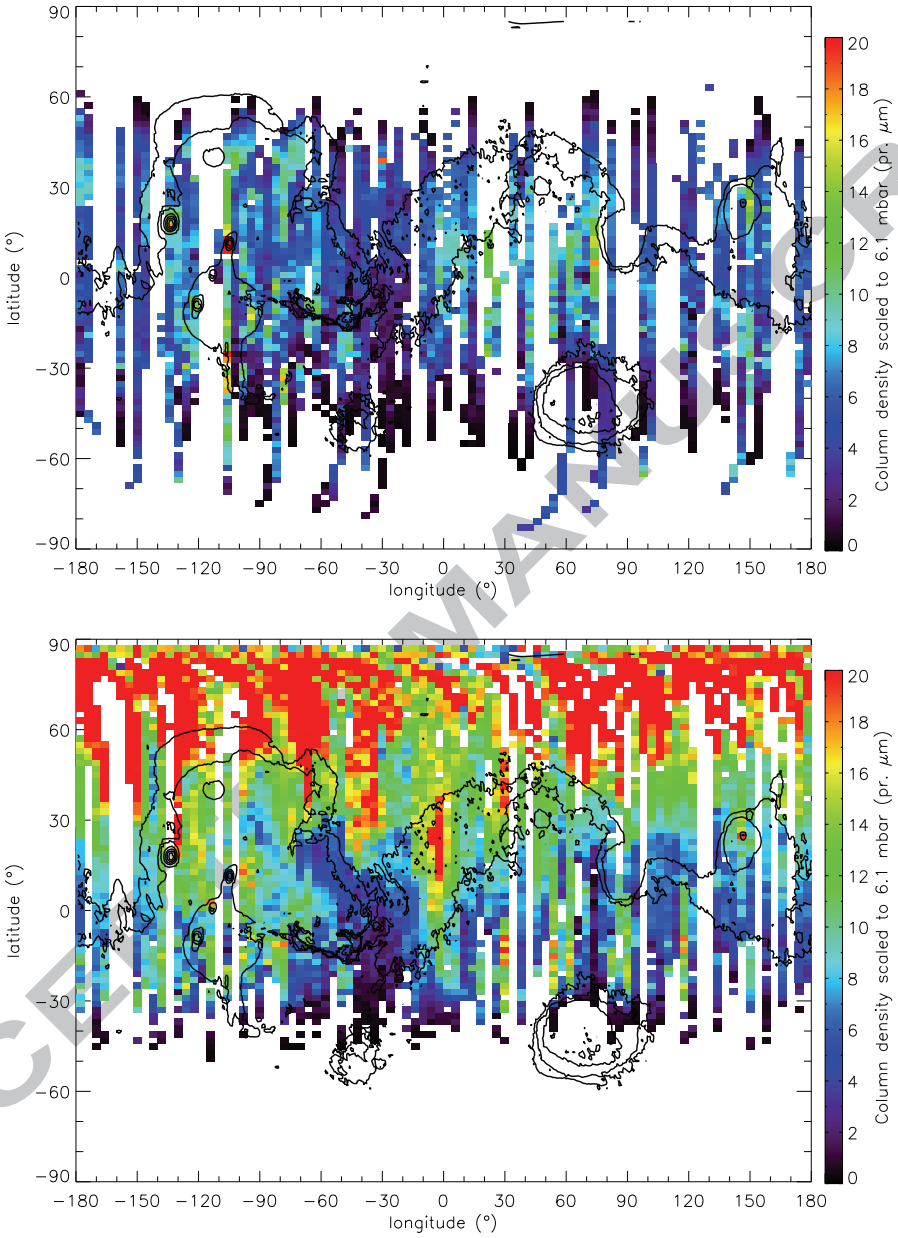

Figure 10: Spatial distribution of water vapor column density during the different seasons. Top: northern spring, $L_s = 330° - 60°$. Bottom: early northern summer, $L_s = 90° - 150°$.

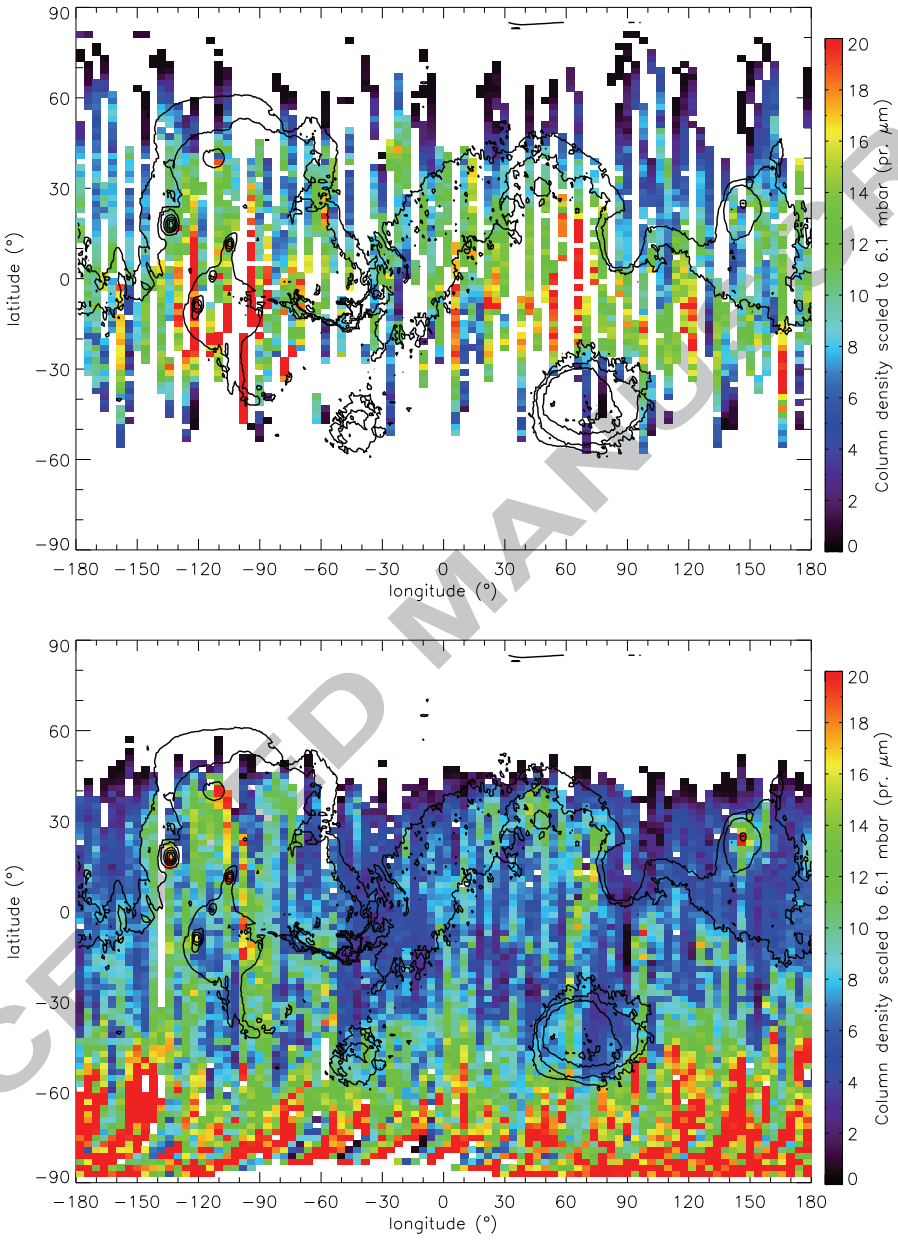

Figure 10: Top: late northern summer and beginning of fall, $L_s = 150° - 200°$. Bottom: northern winter, $L_s = 240° - 360°$.

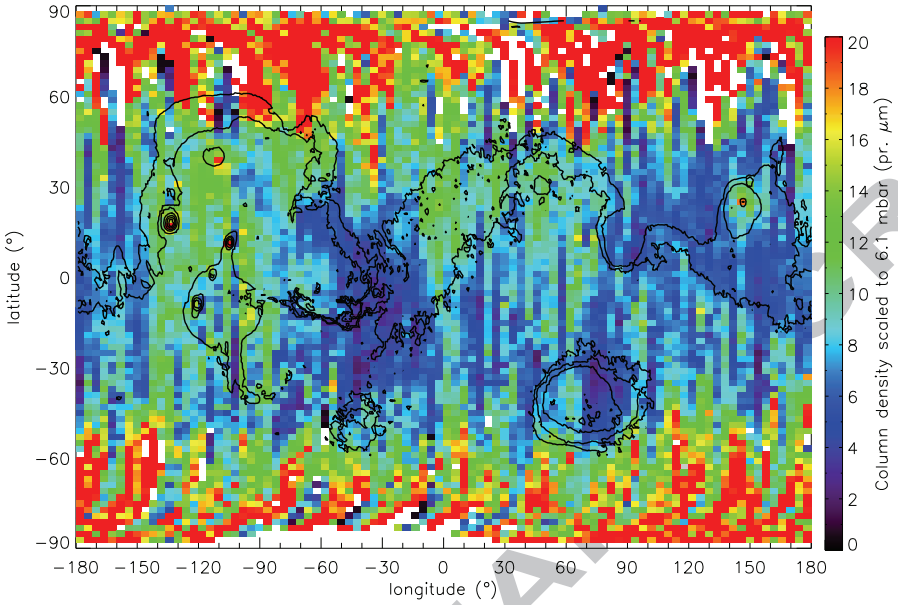

Figure 11: Longitudinal distribution of water vapor considering all the orbits of the first martian year. The column density has been normalized to the zero datum in order to take out the effects of topography.

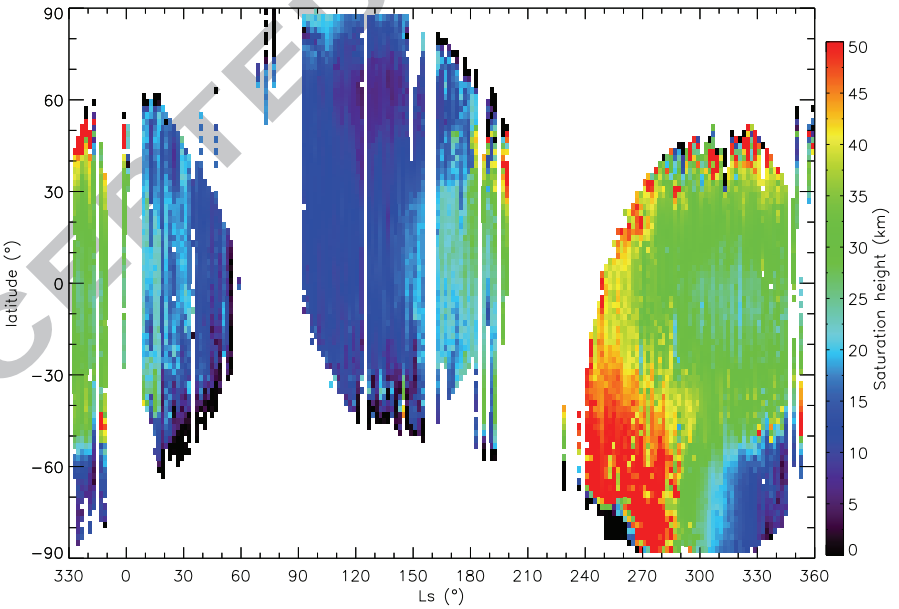

Figure 12: Seasonal trend of the saturation level.

saturation sets in. However, this effect goes in the same direction of the orbital forcing, being the season around aphelion close to the global maximum of the atmospheric water vapor.

The saturation level undergoes a strong annual variation, between $\sim$ 7 and 55 km. During northern spring and summer, especially between $L_s = 30^\circ - 150^\circ$, the level stays between 10 and 15 km, with a minimum below 10 km centered at $L_s = 130^\circ$ and 60° N latitude, whereafter it starts increasing at the equator quite rapidly. Unfortunately the season between $L_s = 180^\circ - 240^\circ$, when we expect the steepest growth, is not covered by measurements. When OMEGA starts acquiring data again, the saturation level is above 40 km everywhere on the planet, with the absolute maximum at $\sim$ 55 km below 45° S, until $L_s \sim 280^\circ$, when saturation has already started to approach the surface again, starting from the equatorial area.

Compared to the seasonal one, all the other dependencies play a minor role. We can however notice that the annual variations are smallest on the equator and get bigger moving towards the poles. This is intuitive, because the amount of insolation undergoes stronger annual variations in the polar areas than at the equator. Moreover, it is at the poles that the seasonal reservoirs of water vapor are concentrated. The results are in good agreement with TES [31], both qualitatively and quantitatively. Regarding the simultaneous measurements from other Mars Express datasets, our results are in good qualitative agreement with both SPICAM (Fedorova, private communication) and PFS-SW (Tschimmel, private communication), which exhibit the same seasonal and latitudinal trend. The agreement with SPICAM is especially significant because a different H_2O band and retrieval method were used. SPICAM tends to find higher values, reaching up to 70 km around the southern summer solstice, while the quantitative agreement with PFS-SW is excellent.

5. Final remarks

We have presented the analysis of water vapor observations performed by OMEGA during the first martian year of Mars Express (MY27). Within the uncertainties, the seasonal trend presents good agreement with earlier observations (MAWD/Viking, TES/MGS) and other Mars Express spectrometers (PFS, SPICAM). Water vapor observations by CRISM in MY28 also are consistent with these results [33]. The main features of the water cycle are common to all experiments. This consistency confirms the current interannual stability of the water cycle of the planet. The inter-Mars Express comparison is especially interesting, because it involves simultaneous observations from three instruments, with different capabilities, using different water vapor spectral bands. The concordance between the results of OMEGA, PFS (in both channels) and SPICAM is a strong argument in favor of their robustness. However, the divergence is more significant in few specific periods, above all during the northern summer maximum. In this case the various datasets differ between each other up to 30 pr. μm. The causes for this discrepancy, which exceeds the retrievals' uncertainties, are not clear.

The main reservoir of atmospheric water is without any doubt the northern polar cap, whose sublimation is the source of the annual maximum of $\sim$ 60 pr. μm at high northern latitudes at the beginning of the local summer. A corresponding, but less

intense, effect is detected on the southern hemisphere. This hemispheric dichotomy is due to the combination of the topographic disparity between the two hemispheres with the current orbital characteristics of Mars (large eccentricity, Earth-like obliquity) [25]. The percentage of water ice in the southern residual polar cap is not negligible [$\approx$ 15%, 1], but it is covered by a thin layer of CO_2 ice all year long, which acts as a perennial cold trap and hampers water sublimation. The main contribution to the southern maximum comes from the seasonal polar cap, which is a minor water reservoir compared to the residual one. OMEGA retrieves a less structured southern maximum than TES or SPICAM.

Other factors are comparatively less important. Circulation plays a role, especially in the equatorward transport from the north pole during summer and the beginning of autumn. However, seasonal water transport signatures from Mars Express measurements seem to be not as strong as older measurements (i.e. not revised TES) suggest. This result is supported by the computations of the total mass of transported water towards the equator during southern summer from PFS-SW measurements [41]. It is difficult to derive strong conclusions on the role of regolith. Both the lack of evident surface-atmosphere exchange signatures and the limited diurnal H_2O fluctuation resulting from the OMEGA-TES comparison seem to suggest that the regolith has only a minor importance for the global water cycle. However, as Fouchet et al. [15] point out in their analysis of PFS-LW data, the regolith can be active and yet involve small absolute quantities of water (3 – 4 pr. μm), which are within our uncertainties. These global surveys contradict some in-situ measurements, that find daily fluctuations up to 10 pr. μm (see Section 4.3). A possible explanation for this discrepancy is the connection between the regolith contribution and local characteristics, as mineralogic composition or the presence of subsurface reservoirs of water, with limited global influence. The new generation of mapping spectrometers is well-suited to investigate water vapor at a regional scale and shed some light on this topic. The study of water behavior on the Tharsis volcanoes by OMEGA suggests the presence of a combination of surface-atmosphere coupling and action by mesoscale circulation in the region, with the latter being dominant [18]. OMEGA also found some daily variability in the south polar region at the end of southern spring ($L_s = 250^\circ - 270^\circ$), which has been attributed mainly to the exchange with the regolith layer [20]. The increase in water vapor during the day is of few pr. μm, also consistent with our results. More dedicated regional studies, complemented by a monitoring of the vertical profile of water vapor within the PBL, are needed to derive a complete picture on the daily variability.

The spatial distribution of scaled H_2O column density is in line with previous measurements, with two planetary maxima over Tharsis and Arabia Terra separated by a strongly depleted region between -60° – -10° E. The Arabia maximum, however, is neither so compact nor so prominent than it appears from other instruments. The rest of the planet is mostly featureless. The longitudinal distribution presents no peculiar seasonal evolution. The two maxima can be seen, more or less evidently, at all seasons. Given the diversity of soil characteristics between Arabia Terra and Tharsis, such a result cannot be considered a proof of the regolith influence on the water cycle by itself, also because some atmospheric models managed to reproduce both maxima by circulation effects alone [15]. Further studies must be performed in order to understand whether the longitudinal distribution of water vapor is controlled by global circulation,

surface-atmosphere exchanges, or a combination of the two. It must be remarked that a rigorous scaling of H_2O column density to take the topography into account depends on the assumptions on the vertical profile of water vapor. The division by the surface pressure, used by every study including the present one, is strictly valid only if water vapor is uniformly mixed up to the end of the atmosphere. In the case of a vertical profile controlled by saturation physics only, such as ours, dividing by the surface pressure is only a zero-order correction, with a residual on the order of p_{sat}/p_0 (where p_{sat} is the pressure at the saturation level and p_0 the surface pressure). From the hydrostatic equation we obtain $p_{sat}/p_0 = e^{-z_{sat}/H}$, with H the pressure scale height. Usually, the height of the saturation level is sufficiently high that this term is negligible and the division by p_0 is a good approximation, with the possible exception of the period around aphelion, when the saturation level is closest to the surface. Further deviations from the well-mixed assumption, not considered in our analysis but suggested by some studies [41, 37], introduce stronger corrections.

The importance of knowing the vertical distribution of water vapor comes out strongly from this discussion. It is necessary not only to remove the topography correctly, but it is also a crucial diagnostics to determine the relative weight of the regolith and of the vertical mixing on the water cycle. Moreover, some contributions to the water cycle can be analyzed in detail only through the water vapor vertical profile. This is the case, for example, of water ice clouds, which appear to be important both from a climatic [26] and a chemical [17] point of view. In our simplified model, retrieving information on the vertical profile of water vapor in the atmosphere means studying the seasonal behavior of the height where saturation sets in. The saturation level varies between $\sim$ 7 and 55 km, with a strong seasonal dependence according to temperature variations during the year. Our results are in good agreement with earlier observations from TES [31] and with simultaneous retrievals from SPICAM and PFS-SW. Direct retrievals of the water vapor vertical profile, however, are strongly needed. The publication of the results from the full SPICAM dataset of solar occultations [of which a limited sample is presented in 9] will allow to make great progress on this crucial diagnostics for the martian water cycle.

Acknowledgements

The authors thank the International Space Science Institute (ISSI) in Bern, to have organized the workshop on “Water in Mars’ Atmosphere: Comparison of Recent Data Sets”. We wish to thank also Mike Smith, Anna Fedorova, Thierry Fouchet, and Martin Tschimmel to have provided their datasets (of TES, SPICAM, PFS-LW, and PFS-SW respectively) for comparison, and Stephen Lewis and an anonymous reviewer for the useful remarks and suggestions to improve the paper.

References

[1] Bibring, J.P., Langevin, Y., Poulet, F., Gendrin, A., Gondet, B., Berthé, M., Soufflot, A., Drossart, P., Combes, M., Bellucci, G., Moroz, V., Mangold, N., Schmitt, B., the OMEGA team, 2004a. Perennial water ice identified in the south polar cap of Mars. Nature 428, 627–630.

[2] Bibring, J.P., Soufflot, A., Berthé, M., Langevin, Y., Gondet, B., Drossart, P., Bouyé, M., Combes, M., Puget, P., Semery, A., Bellucci, G., Formisano, V., Moroz, V., Kottsov, V., Bonello, G., Erard, S., Forni, O., Gendrin, A., Manaud, N., Poulet, F., Poulleau, G., Encrenaz, T., Fouchet, T., Melchiorri, R., Altieri, F., Ignatiev, N., Titov, D., Zasova, L., Coradini, A., Capacionni, F., Cerroni, P., Fonti, S., Mangold, N., Pinet, P., Schmitt, B., Sotin, C., Hauber, E., Hoffmann, H., Jaumann, R., Keller, U., Arvidson, R., Mustard, J., Forget, F., 2004b. OMEGA: Observatoire pour la Minéralogie, l'Eau, les Glaces et l'Activité. pp. 37–49.

[3] Böttger, H., Lewis, S., Read, P., Forget, F., 2005. The effects of the Martian regolith on GCM water cycle simulations. Icarus 177, 174–189.

[4] Clancy, R., Grossman, A., Wolff, M., James, P., Rudy, D., Billawala, Y.N., Sandor, B., Lee, S., Muhleman, D., 1996. Water vapor saturation at low altitudes around Mars aphelion: a key to Mars climate? Icarus 122, 36–62.

[5] Encrenaz, T., Fouchet, T., Melchiorri, R., Drossart, P., Gondet, B., Langevin, Y., Bibring, J.P., Forget, F., Maltagliati, L., Titov, D., Formisano, V., 2008a. A study of the Martian water vapor over Hellas using OMEGA and PFS aboard Mars Express. Astron. Astrophys. 484, 547–553.

[6] Encrenaz, T., Greathouse, T., Richter, M., Bézard, B., Fouchet, T., Lefèvre, F., Montmessin, F., Forget, F., Lebonnois, S., Atreya, S., 2008b. Simultaneous mapping of H_2O and H_2O_2 on Mars from infrared high-resolution imaging spectroscopy. Icarus 195, 547–556.

[7] Encrenaz, T., Melchiorri, R., Fouchet, T., Drossart, P., Lellouch, E., Gondet, B., Bibring, J.P., Langevin, Y., Titov, D., Ignatiev, N., Forget, F., 2005. A mapping of Martian water sublimation during early Northern summer using OMEGA/Mars Express. Astron. Astrophys. 441, L9–L12.

[8] Fedorova, A., Korablev, O., Bertaux, J.L., Rodin, A., Kiselev, A., Perrier, S., 2006. Mars water vapor abundance from SPICAM IR spectrometer: seasonal and geographic distributions. J. Geophys. Res. (Planets) 111, E09S08.

[9] Fedorova, A., Korablev, O., Bertaux, J.L., Rodin, A., Montmessin, F., Belyaev, D., Reberac, A., 2009. Solar infrared occultation observations by SPICAM experiment on Mars-Express: Simultaneous measurements of the vertical distributions of H_2O, CO_2 and aerosol. Icarus 200, 96–117.

[10] Fedorova, A., Rodin, A., Baklanova, I., 2004a. MAWD observations revisited: seasonal behavior of water vapor in the Martian atmosphere. Icarus 171, 54–67.

[11] Fedorova, A., Rodin, A., Baklanova, I., 2004b. Seasonal cycle of water vapor in the atmosphere of Mars as revealed from the MAWD/Viking 1 and 2 experiment. Sol. Syst. Res. 38, 421–433.

[12] Fedorova, A., Trokhimovsky, S., Korablev, O., Montmessin, F., 2010. Viking observation of water vapor on Mars: revision from up-to-date spectroscopy and atmospheric models. Icarus 208, 156–164.

[13] Forget, F., Hourdin, F., Fournier, R., Hourdin, C., Talagrand, O., Collins, M., Lewis, S., Read, P., Huot, J.P., 1999. Improved general circulation models of the Martian atmosphere from the surface to above 80 km. J. Geophys. Res. 104, 24155–24176.

[14] Forget, F., Millour, E., Lebonnois, S., Montabone, L., Dassas, K., Lewis, S., Read, P., López-Valverde, M., González-Galindo, F., Montmessin, F., Lefèvre, F., Desjean, M.C., Huot, J.P., 2006. The new Mars Climate Database, in: Forget, F., Lopez-Valverde, M.A., Desjean, M.C., Huot, J.P., Lefevre, F., Lebonnois, S., Lewis, S.R., Millour, E., Read, P.L., Wilson, R.J. (Eds.), Mars Atmosphere Modelling and Observations, pp. 128–+.

[15] Fouchet, T., Lellouch, E., Ignatiev, N., Forget, F., Titov, D., Tschimmel, M., Montmessin, F., Formisano, V., Giuranna, M., Maturilli, A., Encrenaz, T., 2007. Martian water vapor: Mars Express PFS/LW observations. Icarus 190, 32–49.

[16] Jakosky, B., Farmer, C., 1982. The seasonal and global behavior of water vapor in the Mars atmosphere - Complete global results of the Viking Atmospheric Water Detector experiment. J. Geophys. Res. 87, 2999–3019.

[17] Lefèvre, F., Bertaux, J.L., Clancy, R., Encrenaz, T., Fast, K., Forget, F., Lebonnois, S., Montmessin, F., Perrier, S., 2008. Heterogeneous chemistry in the atmosphere of Mars. Nature 454, 971–975.

[18] Maltagliati, L., Titov, D., Encrenaz, T., Melchiorri, R., Forget, F., Garcia-Comas, M., Keller, H., Langevin, Y., Bibring, J.P., 2008. Observations of atmospheric water vapor above the Tharsis volcanoes on Mars with the OMEGA/MEx imaging spectrometer. Icarus 194, 53–64.

[19] McCleese, D., Schofield, J., Taylor, F., Calcutt, S., Foote, M., Kass, D., Leovy, C., Paige, D., Read, P., Zurek, R., 2007. Mars Climate Sounder: an investigation of thermal and water vapor structure, dust and condensate distributions in the atmosphere, and energy balance of the polar regions. Journal Geophys. Res. (Planets) 112, 5–+.

[20] Melchiorri, R., Encrenaz, T., Drossart, P., Fouchet, T., Forget, F., Titov, D., Maltagliati, L., Altieri, F., Vincendon, M., Langevin, Y., Bibring, J.P., 2009. OMEGA/Mars Express: South Pole Region, water vapor daily variability. Icarus 201, 102–112.

[21] Melchiorri, R., Encrenaz, T., Fouchet, T., Drossart, P., Lellouch, E., Gondet, B., Bibring, J.P., Langevin, Y., Schmitt, B., Titov, D., Ignatiev, N., 2007. Water vapor mapping on Mars using OMEGA/Mars Express. Planet. Space Sci. 55, 333–342.

[22] Michelangeli, D., Toon, O., Haberle, R., Pollack, J., 1993. Numerical simulations of the formation and evolution of water ice clouds in the Martian atmosphere. Icarus 102, 261–285.

[23] Mitrofanov, I., Litvak, M., Kozyrev, A., Sanin, A., Tret'yakov, V., Grin'kov, V., Boynton, W., Shinohara, C., Hamara, D., Saunders, R., 2004. Soil water content on Mars as estimated from neutron measurements by the HEND instrument onboard the 2001 Mars Odyssey spacecraft. Sol. Syst. Res. 38, 253–257.

[24] Montabone, L., Lewis, S.R., Read, P.L., Hinson, D.P., 2006. Validation of martian meteorological data assimilation for MGS/TES using radio occultation measurements. Icarus 185, 113–132.

[25] Montmessin, F., 2006. The Orbital Forcing of Climate Changes on Mars. Space Sci. Rev. 125, 457–472.

[26] Montmessin, F., Forget, F., Rannou, P., Cabane, M., Haberle, R., 2004. Origin and role of water ice clouds in the Martian water cycle as inferred from a General Circulation Model. J. Geophys. Res. (Planets) 109, E10004.

[27] Richardson, M., Wilson, R., 2002. Investigation of the nature and stability of the Martian seasonal water cycle with a General Circulation Model. J. Geophys. Res. (Planets) 107, 5031.

[28] Richardson, M., Wilson, R., Rodin, A., 2002. Water ice clouds in the Martian atmosphere: General Circulation Model experiments with a simple cloud scheme. J. Geophys. Res. (Planets) 107, 5064.

[29] Rizk, B., Haberle, R., Hunten, D., Pollack, J., 1995. Meridional transport and water reservoirs in southern Mars during 1988-1989. Icarus 118, 39–50.

[30] Rodin, A., Korablev, O., Moroz, V., 1997. Vertical distribution of water in the near-equatorial troposphere of Mars: water vapor and clouds. Icarus 125, 212–229.

[31] Smith, M., 2002. The annual cycle of water vapor on Mars as observed by the Thermal Emission Spectrometer. J. Geophys. Res. (Planets) 107, 25.

[32] Smith, M., 2004. Interannual variability in TES atmospheric observations of Mars during 1999-2003. Icarus 167, 148–165.

[33] Smith, M., Wolff, M., Clancy, R., Murchie, S., 2009. Compact Reconnaissance Imaging Spectrometer observations of water vapor and carbon monoxide. J. Geophys. Res. (Planets) 114, 0–+.

[34] Smith, M., Wolff, M., Clancy, R., Spanovich, N., Banfield, D., Ghosh, A., Team, T.A.S., 2006a. Mars exploration rovers Mini-TES observations of boundary layer temperatures and aerosol optical depth, in: Forget, F., Lopez-Valverde, M., Desjean, M., Huot, J., Lefevre, F., Lebonnois, S., Lewis, S., Millour, E., Read, P., Wilson, R. (Eds.), Mars Atmosphere Modelling and Observations, pp. 133–+.

[35] Smith, M., Wolff, M., Spanovich, N., Ghosh, A., Banfield, D., Christensen, P., Landis, G., Squyres, S., 2006b. One Martian year of atmospheric observations using MER Mini-TES. J. Geophys. Res. (Planets) 111, E12S13.

[36] Sprague, A., Hunten, D., Doose, L., Hill, R., Boynton, W., Smith, M., Pearl, J., 2006. Mars atmospheric water vapor abundance: 1991-1999, emphasis 1998-1999. Icarus 184, 372–400.

[37] Tamppari, L., Bass, D., Cantor, B., Daubar, I., Dickinson, C., Fisher, D., Fujii, K., Gunnlauggson, H., Hudson, T., Kass, D., Kleinböhl, A., Komguem, L., Lemmon, M., Mellon, M., Moores, J., Pankine, A., Pathak, J., Searls, M., Seelos, F., Smith, M., Smrekar, S., Taylor, P., Holstein-Rathlou, C., Weng, W., Whiteway, J., Wolff, M., 2010. Phoenix and MRO coordinated atmospheric measurements. J. Geophys. Res. (Planets) 115, E00E17.

[38] Titov, D., 2002. Water vapour in the atmosphere of Mars. Adv. Space Res. 29, 183–191.

[39] Titov, D., Haus, R., 1997. A fast and accurate method of calculation of gaseous transmission functions in planetary atmospheres. Planet. Space Sci. 45, 369–377.

[40] Titov, D., Moroz, V., Grigoriev, A., Rosenqvist, J., Combes, M., Bibring, J.P., Arnold, G., 1994. Observations of water vapour anomaly above Tharsis volcanoes on Mars in the ISM (Phobos-2) experiment. Planet. Space Sci. 42, 1001–1010.

[41] Tschimmel, M., Ignatiev, N., Titov, D., Lellouch, E., Fouchet, T., Giuranna, M., Formisano, V., 2008. Investigation of water vapor on Mars with PFS/SW of Mars Express. Icarus 195, 557–575.

Highlights

> Analysis of the first years of Mars Express data. > Extensive comparison with past and simultaneous measurements. > Agreement between datasets within the uncertainties. > Significant quantitative discrepancies for the northern summer maximum. > Limited amplitude of water vapor diurnal fluctuations.